Proceedings of the Twenty-seventh (2017) International Ocean and Polar Engineering Conference **www.isope.org**
San Francisco, CA, USA, June 25-30, 2017

ISBN 978-1-880653-97-5; ISSN 1098-6189

CFD Simulations of Flows around Finite Stubby Circular Cylinder with Free End

*Jiawei He, Weiwen Zhao, Decheng Wan**
Collaborative Innovation Center for Advanced Ship and Deep-Sea Exploration, State Key Laboratory of Ocean Engineering,
School of Naval Architecture, Ocean and Civil Engineering, Shanghai Jiao Tong University, Shanghai, China
*Corresponding author

ABSTRACT

This study is to investigate flow around a circular cylinder with free end at high Reynolds number (*Re*=43000) by using the technique of Shear-stress transport based detached-eddy simulation (SST-DES). The SST-DES keeps the characteristics of Reynolds-Averaged Navies-Stokes (RANS) in the boundary layer and increases the accuracy of resolution in the regions far away from the wall with Large-Eddy Simulation (LES). Different aspect ratios (namely *L*/*D*) of circular cylinder is firstly simulated in CFD solver naoe-FOAM-SJTU. To further illustrate the vortex shedding characteristics of stationary circular with different aspect ratio, the drag force coefficient and surface pressure coefficient are extensively studied and analyzed. Compared with model tests which are performed by Goncalves et al. (2015), the results of naoe-FOAM-SJTU solver in numerical simulation show that the model in this paper is reliable and efficient.

KEY WORDS: Flow around circular cylinder; Aspect ratios; Free-end effects; SST-DES; naoe-FOAM-SJTU solver.

INTRODUCTION

In the marine and offshore engineering, stubby cylinders (with low aspect ratio) have attracted attention due to the increasing size of the circular platforms, such as spar and monocolumn. The current incidence around these types of platforms promotes the phenomenon of vortex-induced motion (VIM). Recent experimental studies (Gonçalves et al., 2015; Igbalajobi et al., 2013; Iungo et al., 2012; Rostamy et al., 2012) as well as recent numerical simulations (Afgan et al., 2007; Fröhlich and Rodi, 2004; Krajnovic and Krajnović, 2011; Palau-Salvador et al., 2010; Park and Lee, 2000; Rosetti et al., 2013; Rostamy et al., 2013; Zhao et al., 2016), have led to an improved physical understanding of the near-wake vortex flow patterns. Sumner and Heseltine (2008) pointed out the tip vortex structure for a circular cylinder with a free end had a distinctly different from the other cylinders. The sketch provided by Pattenden et al. (2005) in Fig. 1 gives a good overall impression of the experimental findings on the flow characteristics. However, the flow in the vicinity of the free end of finite circular cylinder, and its relationship to near wake, has not been systematically studied. The effects of aspect ratio and boundary layer thickness on the free-end flow field are also not completely understood.

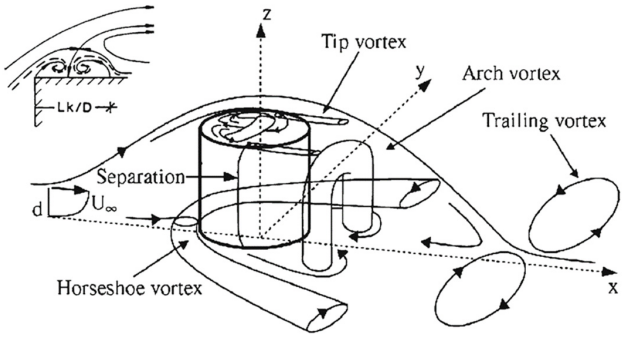

Fig.1 Sketch of flow characteristics of a stubby circular cylinder: (Pattenden et al., 2005)

With the advancement of computer science, Computational Fluid Dynamics (CFD) is playing a crucial role in numerical simulations of turbulent flows. The three common numerical methods for turbulent flows simulation are: Direct Numerical simulation (DNS), Reynolds Averaged Navier-Stokes Simulation(RANS) and Large-Eddy Simulation (LES). DNS and LES are accurate but they are generally expensive at present for many practical industrial applications, with the denser grids and smaller time steps. RANS is commonly used but it is inaccurate to predict massively separated flows. Detached-eddy simulation (DES) was first proposed in 1997 and first used in 1999. DES, as a hybrid RANS/LES method, combines the advantage of RANS and LES. It is designed to automatically turn to a RANS model in boundary layer and a LES subgrid-scale model in massively separation regions. The core idea of DES is to solve respectively the attached flow near wall regions and the rest detached flows shear regions (Menter, 1994). The accuracy of DES predictions for massively separation flow is far superior to that of RANS, and then the cost of DES is far less when compare with LES. Spalart (2009) confirmed that DES solutions with different base RANS models are not sensitive to model choice in the LES region (particularly if separation occurs). Zhao et al. (2016) present a numerical

study of flow over a circular cylinder at high Reynolds number (*Re*=14000) using DES model, which proved to be reliable and efficient.

To investigate flow around a circular cylinder with free end at high Reynolds number (Re=43000), the incompressible finite volume solver naoe-FOAM-SJTU is used for all the computations and DES is selected for turbulence closure. The naoe-FOAM-SJTU is a CFD solver developed based on the open source platform OpenFOAM, aiming at addressing complex ship and ocean engineering flow problems. In addition to the native OpenFOAM libraries, a wave generation and damping module and a 6-degree-of-freedom (6DoF) module were developed. After the two modules are combined with the native OpenFOAM libraries, this solver can be applied not only to the simulations of wave-structure interaction but also to the predictions of motion responses. In the previous work, this solver has been validated for a range of ship and offshore hydrodynamic problems(Cao and Wan, 2015; Shen and Wan, 2014; Zhou et al., 2013). The suitability of the present SST-DES turbulence model has been clarified by Zhao et al for solving flow past two circular cylinders in tandem(Zhao and Wan, 2016b; Zhao et al., 2016). The comparison of SST-URANS and SST-DES have been performed by Zhao and Wan (2016a) using a benchmark case of flow past a circular cylinder at subcritical Reynolds number.

The primary aim of the research described in this paper is to study numerically the flow around a finite stubby circular cylinder with free end. The emphasis is on clarifying the flow field in the wake of the cylinder, particularly near the free end, which is done through DES methods.

TURBULENCE MODELING

SST-DES Model

The version of Menter's SST model implemented in the official OpenFOAM is a modified version rather than the original version. The modification is replacing the vorticity by the invariant measure of the strain rate. The notations in the following paragraphs take the definition in OpenFOAM as standard.

The *k* and *ω* equation are given by:

$$\frac{\partial k}{\partial t}+\frac{\partial(u_j k)}{\partial x_j}=\widetilde{G}-\beta^* k\omega+\frac{\partial}{\partial x_j}\left[(v+\alpha_k v_t)+\frac{\partial k}{\partial x_j}\right] \quad (1)$$

$$\frac{\partial \omega}{\partial t}+\frac{\partial(u_j \omega)}{\partial x_j}=\gamma S^2-\beta\omega^2+\frac{\partial}{\partial x_j}\left[(v+\alpha_\omega v_t)+\frac{\partial \omega}{\partial x_j}\right]+(1-F_1)CD_{k\omega} \quad (2)$$

where, $\widetilde{G}=min(G,c_1\beta^* k\omega)$, and $G=v_t S^2$, F_1 is a blending function which is defined as:

$$F_1=\tanh\left(\arg_1{}^4\right),\ \arg_1=min\left[max\left(\frac{\sqrt{k}}{\beta^*\omega y},\frac{500v}{y^2\omega}\right),\frac{4\alpha_{\omega 2}k}{CD^+_{k\omega}y^2}\right] \quad (3)$$

where, $CD^*_{k\omega}=max\left(CD_{k\omega},10^{-10}\right)$, $CD_{k\omega}=2\alpha_{\omega 2}\cdot\frac{1}{\omega}\frac{\partial k}{\partial x_j}\frac{\partial \omega}{\partial x_j}$

All the constants in transport equations are obtained through blending function F_1

$$\phi=F_1\phi_1+\left(1-F_{1_1}\right)\phi_2 \quad (4)$$

where, ϕ represents α, β and γ in the *k*-*ω* equation.

The eddy viscosity is given by:

$$v_t=\frac{ka_1}{max(a_1\omega,b_1SF_2)} \quad (5)$$

where *S* is invariant measure of the strain rate, define as $S=\sqrt{2S_{ij}S_{ij}}$, and $S_{ij}=\frac{1}{2}\left(\frac{\partial u_i}{\partial x_j}+\frac{\partial u_j}{\partial x_j}\right)$, F_2 is another blending function defined as:

$$F_2=\tanh(\arg_2{}^2),\ \arg_2=max\left(2\frac{\sqrt{k}}{\beta^*\omega y},\frac{500v}{y^2\omega}\right) \quad (6)$$

The constants used here are all the same with reference paper (Zhao and Wan, 2016b).

Menter et al. (2003) modified the *k*-equation by adding a production coefficient F_{DES} to the dissipation term:

$$\frac{\partial k}{\partial t}+\frac{\partial(u_j k)}{\partial x_j}=\widetilde{G}-\beta^* k\omega F_{DES}+\frac{\partial}{\partial x_j}\left[(v+\alpha_k v_t)+\frac{\partial k}{\partial x_j}\right] \quad (7)$$

in which F_{DES} is defined as:

$$F_{DES}=max\left(\frac{l_{RANS}}{C_{DES}\Delta}(1-F_s),1\right) \quad (8)$$

Where, $l_{RANS}=\frac{\sqrt{k}}{\beta^*\omega}$ is the computed turbulent length scale;$\Delta=\sqrt[3]{V}$ is size of sub-grid;

$$l_{DES}=min(C_{DES}\Delta,l_{RANS}) \quad (9)$$

$$C_{DES}=(1-F_1){C_{DES}}^{k-\varepsilon}+F_1{C_{DES}}^{k-\omega} \quad (10)$$

where C_{DES} is the DES constant which is 0.61 here. F_S can be F_1 or F_2, and F_2 is used in this paper.

NUMERICAL TREATMENT

Domain and Grids

The geometry consists of a finite circular cylinder with one end free. The vortices that are shed from the cylinder, along with a strong downwash from its free end require a fairly long computational domain to capture the flow adequately. Four different aspect ratios are selected for numerical investigation, namely *L*/*D*= 0.3, 0.5, 1.0 and 2.0 at Reynolds number of 43000 based on cylinder diameter. where the aspect ratio is defined as $L/D=\frac{\text{submerged length}}{diameter}$, The cylinder diameter is 0.125 *m* and the submerged length is varied to alter the aspect ratios.

The calculation domain (sketched in Fig. 2) spans 20*D* in streamwise direction, 10*D* in lateral and 5.68*D* in vertical direction, respectively. The free-end cylinder is kept constant above the bottom, the distance between the cylinder free end and the channel bottom is around *H*=3.68*D*, i.e. larger than 3.5*D* sufficient for there being no boundary layer effect due to the bottom (Griffith et al., 2011).

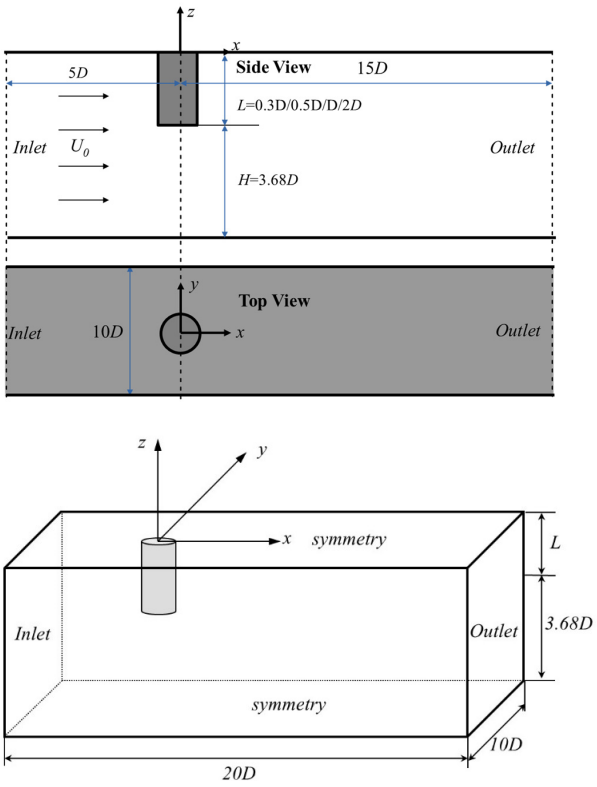

Fig. 2. Sketch of the computational domain

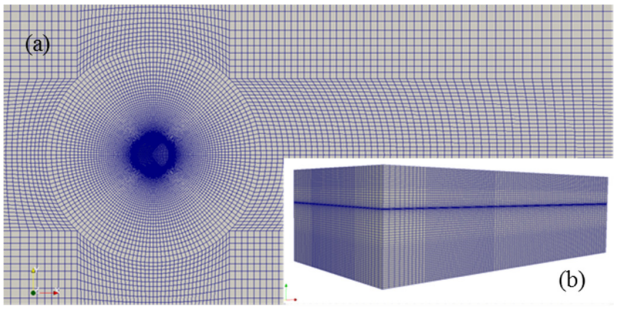

Fig. 3. Details of the grids for the case L/D= 2 (a) View of the numerical domain from the top. Increased cell refinement is located around the cylinder and downstream areas. (b) Overhead view of the numerical domain. Increased cell refinement surrounds the cylinder.

The resulting grids (details of the grids in Fig. 3) yielding a total of 1.52 million grid points for the case L/D = 2. An O-grid type refinement with a diameter of 5D is applied around the cylinder to capture more detailed flow characteristics. Meshes in the vicinity of cylinder free-end are also refined in z-direction. Considering that it is critical setting the first layer thickness under viscous sublayer (the non-dimensioned wall distance y^+ for viscous sublayer is $0<y^+<5$.) to ensure accuracy for high Reynolds number wall-bounded flows. Therefore, in present study the first layer thickness surrounds the cylinder is 0.0002D, corresponding to approximately y^+=5.

Hence, the cross section used in the numerical computations corresponds exactly to the one used in the experiments (Gonçalves et al., 2015). The model is a circular cylinder with aspect-ratio L/D=0.3,0.5,1,2. As Iungo et al. (Iungo et al., 2012) mentioned, the selected aspect-ratio is sufficiently small to guarantee a significant three-dimensional effect of the flow passing over the model free-end on vortex shedding, but still producing a Karman-type wake.

Discretization schemes

The incompressible Navier–Stokes equations, as well as turbulent transport equations, are discretized using a finite volume method. The time discretization is done using second order implicit backward scheme. A second order Gauss integration is used for spatial gradient calculations. The convection operator is discretized using a total variation diminishing (TVD) scheme. The merged PISO-SIMPLE (PIMPLE) algorithm is used for solving the coupled pressure–velocity equations.

RESULTS

Force coefficient

The drag coefficient is given by:

$$C_d = \frac{2F_d}{\rho LDU^2} \tag{11}$$

Where ρ is the density, F_d is the time average drag force, U is the velocity of flow.

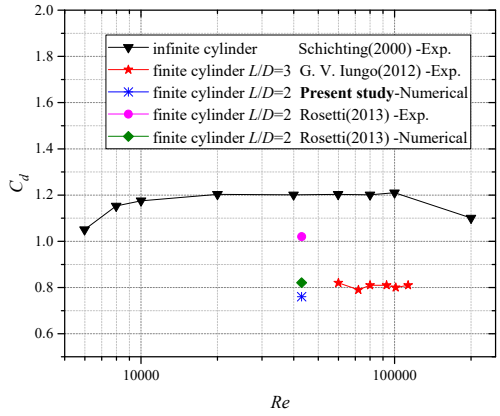

Fig.4. Drag coefficients from numerical calculations and experiments

Table 1. The relationship between drag coefficient and aspect ratio from the present work as well as previous work from the literature

The origin of data	L/D	Re	C_d	Relative difference (%)
Present study	L/D=0.3	43000	0.58	17.14%
	L/D=0.5		0.61	18.66%
	L/D=1		0.72	23.40%
	L/D=2		0.76	25.49%
R.T.Gonçalves(2015)	L/D=0.3	43000	0.7	-
	L/D=0.5		0.75	-
	L/D=1		0.94	-
	L/D=2		1.02	-

Fig. 4 show the relationship between mean drag coefficient and aspect

ratio from the present work as well as previous work from numerical calculations and the experiment. The black line with down-pointing triangle markers show experimental values from Schlichting and Shapiro (2000) for infinite cylinder, which evidently excludes free-tip or free surface effects. The red line with star markers shows experimental values from Iungo et al (2012) for the finite cylinder L/D=3. Two previously values by Rosetti et al (2013) for Re = 43000 and L/D=2 are show as a reference. The result identified as L/D=2 corresponds to the drag coefficient for the present case, Re =43000 and L/D=2.

Table 1 show the relationship between mean drag coefficient and aspect ratio from the present work the experiment by Gonçalves et al.(2015). In spite of the inaccurate drag coefficient, the variation tendency that a decrease in drag force coefficients with decreasing aspect ratio are consistent with Gonçalves' PIV experiments. Moreover, the drag coefficient for this case is somewhat lower than that of the infinite cylinder, which is consistent with what is found in the literature(Sumner et al., 2004).

There is an evident poor comparison between experimental and numerical results. A possible explanation for the inaccuracy is the current study neglected free surface effect. We can see the paper's (Rosetti et al., 2013) result obtained with a free surface condition is much more comparable to the experimental value, showing that the free-surface seems to be more important in this case with regards to drag forces. A simulation with free surface will be addressed in future work.

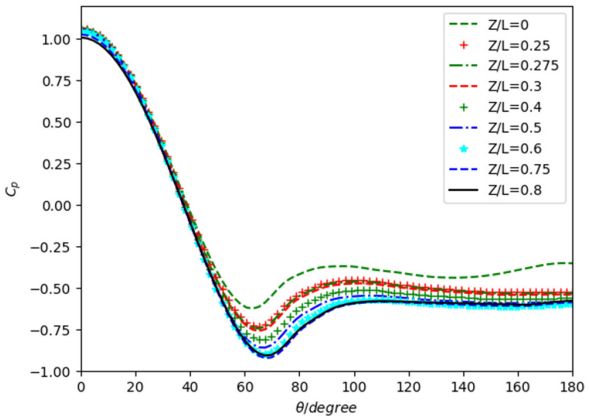

Fig. 5. Mean surface pressure coefficient distribution of the finite cylinder in the horizontal plane at different z/L (L=2D case)

Fig. 5. shows the mean surface pressure coefficient distribution of the finite cylinder in the horizontal plane at different z/L. The angle θ is measured from the upstream face of the cylinder. Starting from the curve corresponding to $60° \leqslant \theta \leqslant 80°$, the absolute value of C_p is observed decreasing with the increasing of the z/L. This characteristic can be attributed to the upwash generated by the flow passing over the free-end. whereas for the reduced C_p can be considered an effect of the velocity field induced by the small horse-shoe vortex that is probably present in that region. Moving to higher values of θ, a lower C_p is generally detected in the vicinity of cylinder free-end, also due to the induced upwash.

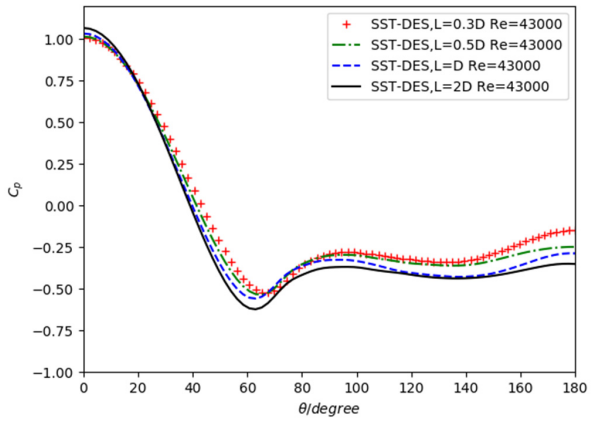

Fig. 6. Mean surface pressure coefficient distribution of the finite cylinder in the horizontal plane at z=0 with different aspect-ratio L/D

Fig. 6 shows the mean surface pressure coefficient C_p, around the condition of the cylinder with different aspect-ratio L/D=0.3,0.5,1.0,2.0. The angle θ is measured from the stagnation point of the cylinder.

The curve corresponding to θ suggests that the flow detachment over the lateral surface occurs at increasing aspect ratio. With the vary of aspect ratio L/D=0.3,0.5,1.0,2.0, the lowest value of C_p is coming at θ=77°, 72°, 67°, 61°respectively. The lower degree of θ means the earlier separation of flow. Therefore, it is found that higher aspect ratio means earlier separation of flow. It is probably caused by the downwash trailing vortex induced by rushed detachment for higher heights free end.

Instantaneous vorticity

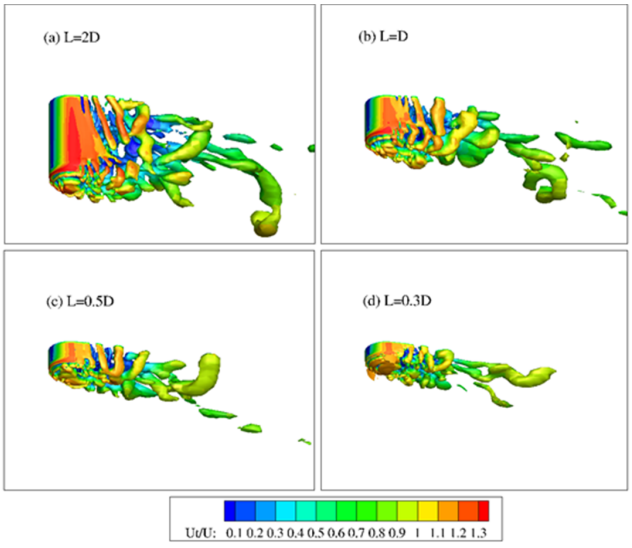

Fig. 7. Instantaneous isosurface of vorticity Q=6, dye visualization with non-dimensioned velocity magnitude

Fig. 7 shows the instantaneous isosurface of vorticity Q=6, dye visualization with non-dimensioned velocity magnitude. The definition of Q is given by:

$$Q = \frac{1}{2}\left(|\Omega|^2 - |S|^2\right) \tag{12}$$

where S is invariant measure of the strain rate tensor, define as $S = \sqrt{2S_{ij}S_{ij}}$, and $S_{ij} = \frac{1}{2}\left(\frac{\partial u_i}{\partial x_j} + \frac{\partial u_j}{\partial x_j}\right)$, Ω is invariant measure of vorticity tensor.

As shown in Fig. 7, the vortex shedding is visible in downstream. The separated flow coming from the free end interacts with the separated flow along the cylinder and delays the separation. For the four cases of cylinder with different aspect-ratio L/D=0.3,0.5,1,2. The strong downwash can all be clearly seen due to the existence of free end. Vortex shedding for cylinders with different aspect-ratio are all suppressed in the top region rear to the free end. While the vortex structures of cylinder varies for different aspect-ratio. The wake region gets narrow and chaotic with decreasing aspect ratio, and the low aspect ratio (L/D $\leqslant$0.5) may be similar to the flow around a hemisphere.

Contours of velocity

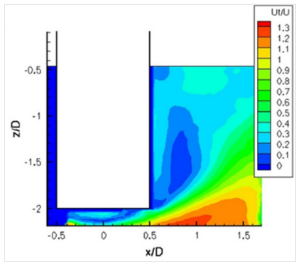

(a) L/D=2.0 _Exp. by Gonçalves

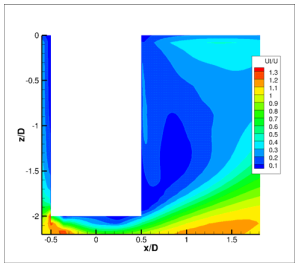

(a) L/D=2.0 Present numerical

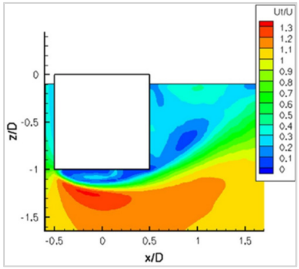

(b) L/D=1.0 Exp. by Gonçalves

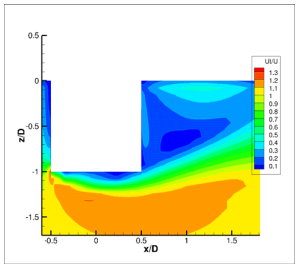

(b) L/D =1.0 Present numerical

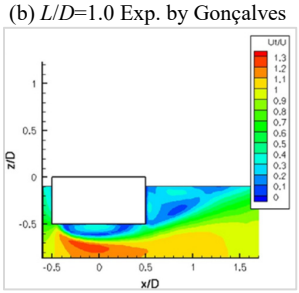

(c) L/D=0.5 Exp. by Gonçalves

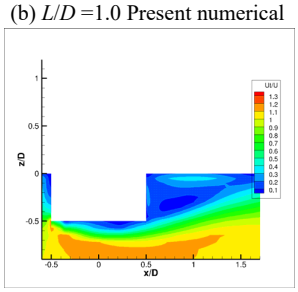

(c) L/D=0.5 Present numerical

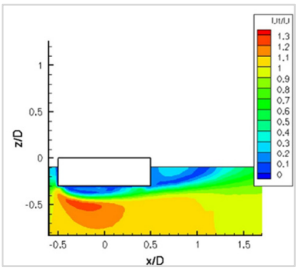

(d) L/D =0.3 Exp. by Gonçalves

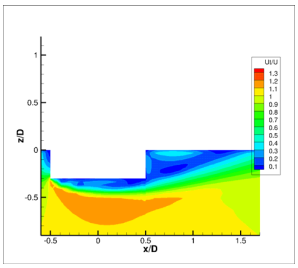

(d) L/D =0.3 Present numerical

Fig. 8. Contours of mean total velocity U_t/U in the vertical center plane at y/D=0 for Re=43000 (a) L/D=2.0, (b) L/D =1.0, (c) L/D =0.5 and (d) L/D =0.3. (The left column figures are PIV experimental results by Gonçalves et al. (2015), the right column figures are my SST-DES numerical simulation results.)

Fig. 8 shows the contours of mean total velocity U_t/U in the vertical center plane at y/D=0 for cylinders with L/D=2.0, 1.0, 0.5 and 0.3. Compare the contours of mean total velocity between experiment and CFD, rough agreement is found between my SST-DES and the experiments of PIV (Gonçalves et al., 2015) for the mean flow behavior. The drastic downwash can be seen in the free end region rear the cylinder. The end effects are observed in these plots, with a strong recirculation extending from the bottom of the cylinder. The visualizations showed two recirculation regions: the first one over the cylinder free end, and the second one behind the cylinder.

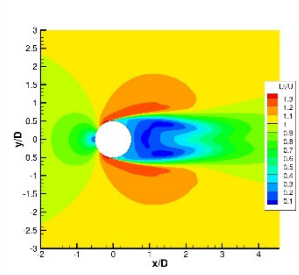

(a) L/D=2.0

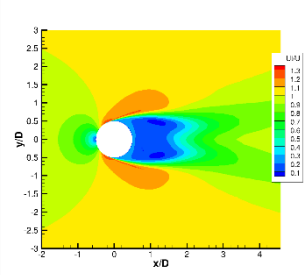

(b) L/D =1.0

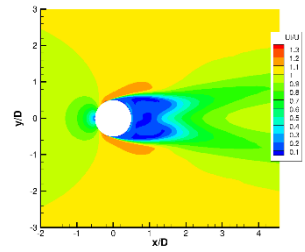

(c) L/D =0.5

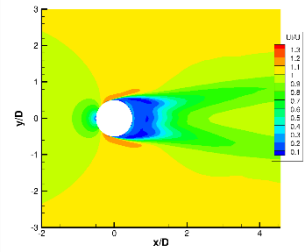

(d) L/D =0.3

Fig. 9. Contours of mean total velocity U_t/U in the horizontal plane, z/L=-0.5 for Re=43000 (a) L/D=2.0, (b) L/D =1.0, (c) L/D =0.5 and (d) L/D =0.3.

Fig. 9. shows the contours of mean total velocity U_t/U in the horizontal plane at z/L=-0.5 for Re=43000 (a) L/D=2.0, (b) L/D =1.0, (c) L/D =0.5 and (d) L/D =0.3. The figures show a symmetrical pair of vortices, which is in accordance with the conclusions of Yu et al. (Yu et al., 2008). Regular vortex shedding from the cylinder seems to be suppressed and

the vortex formation region is barely distinguishable in the region near the free end with low aspect ratio. The flow around very low aspect ratio cylinder ($L/D \leqslant 0.5$) may be similar to the flow around a hemisphere. which can be seen in Rosetti et al (2013).

CONCLUSIONS

The present work uses SST-DES to investigate the trailing vortex near the free end of a circular cylinder. The results showed a decrease in drag force coefficients with decreasing aspect ratio. As Palau Palau-Salvador et al. (2010) mentioned, "the vortex shedding flow past very long cylinders is significantly complicated further by end effects, but mainly by those of the free end.". Herein, with present SST-DES numerical model, we can also observe the free end effects on finite stubby circular cylinder (L/D=2.0, 1.0, 0.5 and 0.3). The flow over the free end descends past the cylinder, forming a longitudinal recirculation region accompanied by a pair of tip vortices originating from the trailing edge of the free end. Overall, rough good agreement is found between SST-DES and the experiments of PIV (Gonçalves et al., 2015) for the mean flow behavior. This demonstrates that SST-DES is a suitable and economical method for simulating flows as complex as the ones investigated. Finally, the results for the stubby finite cylinder provide important basic information and guidance for attempts to calculate the even more complex also important situations of SPAR platforms.

ACKNOWLEDGEMENTS

This work is supported by the National Natural Science Foundation of China (51379125, 51490675, 11432009, 51579145), Chang Jiang Scholars Program (T2014099), Shanghai Excellent Academic Leaders Program (17XD1402300), Shanghai Key Laboratory of Marine Engineering (K2015-11), Program for Professor of Special Appointment (Eastern Scholar) at Shanghai Institutions of Higher Learning (2013022), Innovative Special Project of Numerical Tank of Ministry of Industry and Information Technology of China(2016-23/09) and Lloyd's Register Foundation for doctoral student, to which the authors are most grateful.

REFERENCES

Afgan, I, Moulinec, C, Prosser, R, and Laurence, D (2007). "Large eddy simulation of turbulent flow for wall mounted cantilever cylinders of aspect ratio 6 and 10," *Int J Heat Fluid Flow*, 28(4), 561–574.

Cao, H, and Wan, DC (2015). "Development of Multidirectional Nonlinear Numerical Wave Tank by Naoe-FOAM-SJTU Solver," *J Adv Res Ocean Eng*, 1(1), 14–24.

Fröhlich, J, and Rodi, W (2004). "LES of the flow around a circular cylinder of finite height," *Int J Heat Fluid Flow*, 25(3), 537–548.

Gonçalves, RT, Franzini, GR, Rosetti, GF, Meneghini, JR, and Fujarra, ALC (2015). "Flow around circular cylinders with very low aspect ratio," *J Fluids Struct*, 54, 122–141.

Griffith, MD, Leontini, J, Thompson, MC, and Hourigan, K (2011). "Vortex shedding and three-dimensional behaviour of flow past a cylinder confined in a channel," *J Fluids Struct*, 27(5–6), 855–860.

Igbalajobi, A, McClean, JF, Sumner, D, and Bergstrom, DJ (2013). "The effect of a wake-mounted splitter plate on the flow around a surface-mounted finite-height circular cylinder," *J Fluids Struct*, 37, 185–200.

Iungo, GV, Pii, LM, and Buresti, G (2012). "Experimental investigation on the aerodynamic loads and wake flow features of a low aspect-ratio circular cylinder," *J Fluids Struct*, 28, 279–291.

Krajnovic, S, and Krajnović, S (2011). "Flow around a tall finite cylinder explored by large eddy simulation," *J Fluid Mech*, 676(2011), 294–317.

Menter, FR (1994). "Two-equation eddy-viscosity turbulence models for engineering applications," *AIAA J*, 32(8), 1598–1605.

Palau-Salvador, G, Stoesser, T, Fröhlich, J, Kappler, M, and Rodi, W (2010). "Large Eddy Simulations and Experiments of Flow Around Finite-Height Cylinders," *Flow, Turbul Combust*, 84(2), 239–275.

Park, C-WW, and Lee, S-JJ (2000). "Free end effects on the near wake flow structure behind a finite circular cylinder," *J Wind Eng Ind Aerodyn*, 88(2–3), 231–246.

Pattenden, RJ, Turnock, SR, and Zhang, X (2005). "Measurements of the flow over a low-aspect-ratio cylinder mounted on a ground plane," *Exp Fluids*, 39(1), 10–21.

Rosetti, GF, Vaz, G, Hoekstra, M, Gonçalves, RT, and Fujarra, ALC (2013). "CFD Calculations for Free-Surface-Piercing Low Aspect Ratio Circular Cylinder With Solution Verification and Comparison With Experiments," *Vol 7 CFD VIV*, (JUNE), V007T08A056.

Rostamy, N, Sumner, D, Bergstrom, DJ, and Bugg, JD (2012). "An Experimental Study of the Flow Above the Free Ends of Surface-Mounted Bluff Bodies," *Vol 1 Symp Parts A B*, 981.

Rostamy, N, Sumner, D, Bergstrom, DJ, and Bugg, JD (2013). "Instantaneous flow field above the free end of finite-height cylinders and prisms," *Int J Heat Fluid Flow*, 43, 120–128.

Shen, Z, and Wan, D (2014). "Computation of Steady Viscous Flows around Ship with Free Surface by Overset Grids Techniques in OpenFOAM," 3, 832–838.

Spalart, PR (2009). "Detached-Eddy Simulation," *Annu Rev Fluid Mech*, 41(1), 181–202.

Sumner, D, and Heseltine, JL (2008). "Tip vortex structure for a circular cylinder with a free end," *J Wind Eng Ind Aerodyn*, 96(6–7), 1185–1196.

Sumner, D, Heseltine, JL, and Dansereau, OJP (2004). "Wake structure of a finite circular cylinder of small aspect ratio," *Exp Fluids*, 37(5), 720–730.

Yu, G, Avital, EJ, and Williams, JJR (2008). "Large Eddy Simulation of Flow Past Free Surface Piercing Circular Cylinders," *J Fluids Eng*, 130(10), 101304.

Zhao, W-W, and Wan, DC (2016a). "Numerical study of 3D flow past a circular cylinder at subcritical Reynolds number using SST-DES and SST-URANS," *Shuidonglixue Yanjiu Yu Jinzhan/Chinese J Hydrodyn Ser A*, 31(1).

Zhao, W, and Wan, DC (2016b). "Benchmark for Detached-Eddy Simulation of Flow Past Tandem Cylinders," *Elev Asian Comput Fluid Dyn Conf Sept 16-20, 2016, Dalian, China*, 397–401.

Zhao, W, Wan, DC, and Sun, R (2016). "Detached-Eddy Simulation of Flows over a Circular Cylinder at High Reynolds Number," *Proc Twenty-Sixth Int Ocean Polar Eng Conf*, 96(10–11), 1528–1536.

Zhou, H, Cao, H, and Wan, DC (2013). "Numerical predictions of wave impacts on the supporting structures of shanghai donghai-bridge offshore wind turbines," *Proc Int Offshore Polar Eng Conf*, 9, 216–224.